Multi-transmitter ship target detection technique with GNSS-based passive radar

F. Pieralice*, D. Pastina*, F. Santi*, M. Bucciarelli†

** Department of Information Engineering, Electronics and Telecommunications, University of Rome "La Sapienza" Rome, Italy*
† Sympas s.r.l., Viale Giulio Cesare 71, Rome, Italy

Keywords: moving target detection, passive radar, GNSS-based radar, multi-transmitter

Abstract

The exploitation of the Global Navigation Satellite Systems (GNSS) as transmitters of opportunity in passive radar systems for maritime surveillance is particularly attractive because of the main advantages consisting in a global coverage (even in open sea) and in the availability of multiple sources (different satellites and constellations). The main drawback stays in the restricted power budget provided by navigation satellites. This characteristic makes necessary to conceive, define and develop detection techniques able to overcome such limitation. To this aim this work proposes a range-Doppler domain processing technique able to integrate over long time intervals the returns from a moving target illuminated by multiple GNSS transmitters. Several examples are shown to demonstrate the effectiveness of the proposed approach.

1 Introduction

The alternative utilization of Global Navigation Satellite Systems (GNSS) for remote sensing applications has been intensively investigated since many years. A number of well-established systems to remotely sense has been investigated in the field of the GNSS reflectometry (GNSS-R) [1]. In the field of radar sensors, GNSS have been successfully employed in passive bistatic and multistatic Synthetic Aperture Radar, providing a powerful tool for persistent Earth observation and monitoring[2]-[5].

In the framework of passive radar systems for maritime surveillance, GNSS are one of the few choices assuring global coverage (even in open sea). In [6] the system concept has been presented and the feasibility of using the GNSS reflected signal to detect maritime moving targets has been experimentally demonstrated. However one of the biggest issues of GNSS for passive radar applications is the low level of power density reaching the Earth surface [7]. Therefore innovative processing techniques specified tailored for the GNSS passive radar have to be developed. In particular in [8] a long integration time technique has been proposed able to concentrate the signal energy over processing intervals long enough (tens of seconds) to retrieve signal to disturbance levels suitable for the detection.

A further performance improvement could be obtained by exploiting the inherent multistatic nature of GNSS-based (GPS, Glonass, Galileo, BeiDou) passive radar. Indeed, at any time of the day, there are 6-8 satellites in a single constellation (24-32 with all 4 GNSS constellations fully operational) illuminating any point on Earth from different angles. All of these signals could be received by a single receiver and jointly processed to improve system performance [4][5]. To this aim, starting from the technique in [8], this work proposes a new multistatic range-Doppler processing technique able to cope with long integration times and multiple transmitters.

The paper is organized as follows: an overview of the system is given in Section II and the proposed multi-transmitter processing technique is described in Section III. Results on synthetic datasets are shown in Section IV while Section V reports some conclusions.

2 System overview

A general configuration of the GNSS-based radar used in maritime surveillance is depicted in Fig. 1.

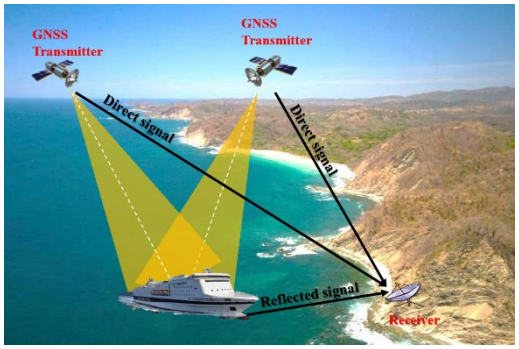

Fig. 1. System concept for GNSS-based radar for maritime surveillance.

GNSS satellites are used as transmitting sources and a receive-only device (mounted on the coast or on a sea buoy) is equipped with two channels: the reference channel, recording the direct satellite signals to provide signal synchronisation, and the surveillance channel, collecting the reflections from the surveyed area. Since GNSS operate with frequency or code division approaches, the receiver is able to separate the signals pertaining to the different satellites. The local (O, X, Y, Z) reference system is depicted in Fig. 2. It is obtained by a rotation of the East-North-Up (ENU) reference system centred in the receiver position, where the x-axis represents the direction on which the beam of the surveillance antenna is pointed.

The target and the transmitters trajectories during the observation time T (usually several tens or hundreds of seconds long) are defined in that local reference system, while the

receiver position is fixed at the centre of it. The instantaneous distance among the i-th (i=1,…, N_{Tx}) transmitter (Tx), receiver (Rx) and target (Tg) are defined as follows: $R_{Tx_i-Tg}(t)$ is the i-th transmitter to target distance, $R_{Tg-Rx}(t)$ is the target to receiver distance and $R_{Tx_i-Rx}(t)$ is the i-th transmitter to receiver baseline, where t is slow time defined in the interval $[-T/2, T/2]$. The transmitter and target vector positions are also defined by the following angles: ϕ_{Tx_i} is the clockwise angle on x-y plane between x-axis and the satellite projection on x-y plane, θ_{Tx_i} is the out-of-plane angle between the x-y plane and the satellite, ϕ_{Tg} is the clockwise angle between x-axis and target direction.

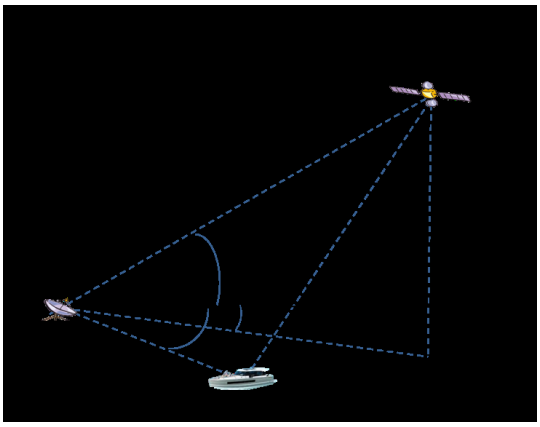

Fig. 2. Local reference system.

Accounting for a compensation of the instantaneous baseline, the bistatic target range is defined as

$$r_i(t) = R_{Tx_i-Tg}(t) + R_{Tg-Rx}(t) - R_{Tx_i-Rx}(t) \quad (1)$$

and bistatic target Doppler frequency is

$$f_i(t) = -\frac{1}{\lambda}\dot{r}_i(t) \quad (2)$$

being λ the wavelength of the transmitted signal.

After quadrature demodulation and radar data reformatting according to an equivalent Pulse Repetition Interval (PRI) typically set to the duration of the ranging code, for each considered transmitter the surveillance channel signal can be compressed by a correlation with a noise-free replica of the reference signal, which can be regenerated according to the tracked direct signal parameters, [6]. The range-compressed data in the fast-time&slow-time are then provided in input to the processing chain introduced in the following section.

3 Multi-transmitter detection technique

The proposed technique, sketched in Fig. 3, aims at exploiting the available satellites to enhance the detection performance with respect to that achievable with the single transmitter. Since the range and Doppler target position in the basic plane depends on considered transmitter, range-Doppler maps coming from the different baselines cannot be directly combined and a proper technique is needed to allow the integration of the different target returns.

The overall processing chain, performing the integration on long time intervals and on multiple transmitters, comprises four steps:

1. Sequence of RD maps formation – The range compressed data pertaining to each transmitter is segmented in N consecutive batches of limited time duration T_b such that constant reflectivity and negligible range and Doppler migration can be assumed. A FFT in the slow-time dimension is applied to each batch to obtain a sequence of N RD maps.

2. Target Motion Compensation (TMC) – TMC basically compensates the range and Doppler migration of the target in the sequence of the N RD maps to allow the integration of the target returns of the entire dwell time, [8]. This is done separately for each baseline. Let RD_i^n (n= $-\frac{N}{2}, \dots, \frac{N}{2}-1$) be the n-th RD map, referring to central time $t_n = nT_b + \frac{T_b}{2}$ and to the i-th transmitter: in such map the moving target is located in $\left(r_i^{t_n}, f_i^{t_n}\right)$. The range and Doppler migrations experienced with respect to the position (r_i^0, f_i^0) at the reference time t=0 can be written as

$$\Delta r_i^{t_n}\left(f_i^{t_n}, \dot{f}_i^*\right) = r_i^{t_n} - r_i^0 = \\ = -\lambda\left[\left(f_i^{t_n} - \dot{f}_i^* t_n\right)t_n + \dot{f}_i^* \frac{(t_n)^2}{2}\right] \quad (3)$$

$$\Delta f_i^{t_n}\left(\dot{f}_i^*\right) = f_i^{t_n} - f_i^0 = \dot{f}_i^* t_n. \quad (4)$$

being $\dot{f}_i^*$ the target Doppler rate assumed constant during the dwell time. Therefore, range migration can be compensated by multiplying the map in the (range frequency, Doppler frequency) domain for a phase term according to eq. (3), where the range frequency domain is obtained applying a FFT along the range dimension, whereas the Doppler migration is corrected in the (range, slow-time) domain by the phase term corresponding to eq. (4).

3. Multistatic compensation – Due to the different transmitter positions, the target will be differently located in the different RD maps. Therefore, the aim of this step is to align the target contributions concerning the different transmitters to allow a proper integration. The following assumptions are made by the proposed multistatic compensation technique:

a) The receiver only determines the target Doppler rate, namely the same value can be assumed for all the baselines $\dot{f}_i^* \equiv \dot{f}^* \ \forall i$. This is a consequence of the considered acquisition geometry implying a considerable distance between the transmitters and the target.

b) The range between the transmitters and the receiver ($R_{Tx_i-Rx}\ i = 1, \dots, N_{Tx}$) is much larger than the size of the area to be surveyed.

Starting from these assumptions and referring to acquisition geometry in Fig. 2, we can obtain the following approximate expressions for the differential bistatic range

$$r_i = R_{Tx_i-Tg} + R_{Tg-Rx} - R_{Tx_i-Rx} \\ \cong R_{Tg-Rx}\left(1 - \cos\theta_{Tx_i}\cos\left(\phi_{Tx_i} - \phi_{Tg}\right)\right) \quad (5)$$

and Doppler frequency

$$f_d^i = -\frac{1}{\lambda}\dot{r}_i = -\frac{1}{\lambda}\dot{R}_{Tg-Rx}\left(1+\cos\theta_{Tx_i}\cos\left(\phi_{Tx_i}-\phi^*_{Tg}\right)\right)^{A}$$
$$-\frac{1}{\lambda}R_{Tg-Rx}\sin\theta_{Tx_i}\cos\left(\phi_{Tx_i}-\phi^*_{Tg}\right)\dot{\theta}_{Tx_i}^{B}$$
$$-\frac{1}{\lambda}R_{Tg-Rx}\cos\theta_{Tx_i}\sin\left(\phi_{Tx_i}-\phi^*_{Tg}\right)\dot{\phi}_{Tx_i}^{C}$$
$$+\frac{1}{\lambda}R_{Tg-Rx}\cos\theta_{Tx_i}\sin\left(\phi_{Tx_i}-\phi^*_{Tg}\right)\dot{\phi}^*_{Tg}^{D}$$
$$= f_d^A + f_d^B + f_d^C + f_d^D \quad (6)$$

being ϕ^*_{Tg} and $\dot{\phi}^*_{Tg}$ the direction of arrival of the target with respect to the receiver (Fig. 2) and its derivative. On the basis of the above model the proposed multistatic compensation comprises three steps:

i. Range axis scaling – The scale of range axis is done according to the scale factor:

$$\frac{1}{1-\cos\theta_{Tx_i}\cos\left(\phi_{Tx_i}-\phi^*_{Tg}\right)} \quad (7)$$

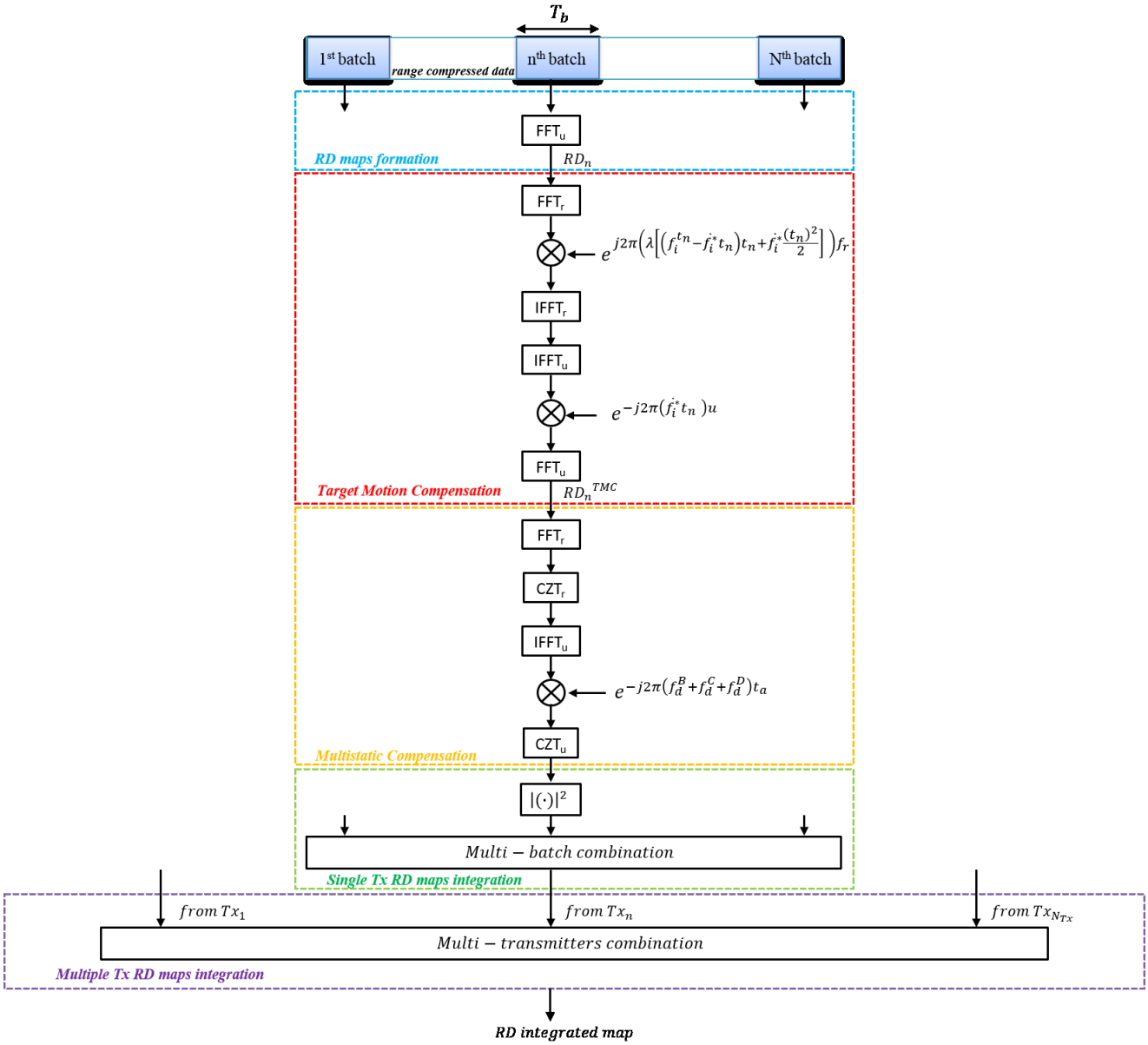

Fig. 3. Multistatic range-Doppler processing technique scheme.

After this step the target is located at range bin corresponding to R_{Tg-Rx}. Such scaling can be easily implemented through a chirp-z transform in the fast time dimension.

ii. Doppler shift compensation – The f_d^B, f_d^C, f_d^D Doppler components are compensated by multiplying the i-th map in the (range, slow time) domain by the corresponding phase terms.

iii. Doppler axis scaling – The scale of Doppler axis is done according to the scale factor:

$$\frac{1}{1-\cos\theta_{Tx_i}\cos\left(\phi_{Tx_i}-\phi_{Tg}^*\right)} \tag{8}$$

After this step the target is located at Doppler bin corresponding to $-\frac{1}{\lambda}\dot{R}_{Tg-Rx}$. Such scaling can be easily implemented through a chirp-z transform in the slow time dimension.

4. RD maps integration – After the multistatic compensation procedure, the target is located in the same position in all the maps so that its returns can be properly integrated.

The procedure described above depends on the specific target Doppler rate $\dot{f}^*$, on the angle of arrival ϕ_{Tg}^* and on its derivative $\dot{\phi}_{Tg}^*$. A completely adaptive technique can be obtained by considering a bank structure with different values of the above parameters. Particularly up to the first step of the multistatic compensation only adaptation to the Doppler rate is required while the last two steps of the multistatic compensation depend also on the angular values. This allows to cope with the multi-transmitter case while at the same time keeping the computational load under control.

The parameters of the best fitting branch of the bank provide also a direct estimate of the target cross-range velocity component and direction of arrival. Therefore this method can be exploited to design a joint detection and localization technique.

4 Simulated results

A preliminary simulated analysis is here proposed to verify the effectiveness of the proposed technique. Three GPS transmitters are considered as illuminators of opportunity and a target moves in the surveyed area. The target and the transmitters trajectories, in the local reference system of Fig. 2, are reported in Fig. 4 and Fig. 5 providing a top view of the considered acquisition geometry. At the reference instant t=0 the target is along the radar Line-of-Sight (LOS) at a distance of 1000m, moving with a velocity of 10kt with heading angle 135° (measured counter-clockwise from the LOS direction). T is set to 30s and this interval is segmented in N = 15 batches 2 secs each. The parameters used for generation of the synthetic datasets are reported in Table 1. An additive white Gaussian noise occupying the useful signal bandwidth has been considered as disturbance background, which results in a SNR after matched filtering for range compression equal to -26.6 dB, namely very challenging conditions. Considered conditions and values are well in line with evidence from experimental trials [6][8].

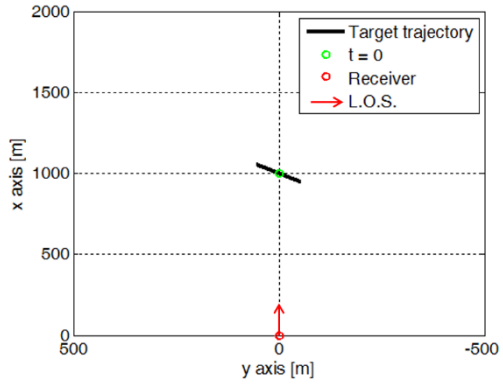

Fig. 4. Target trajectory.

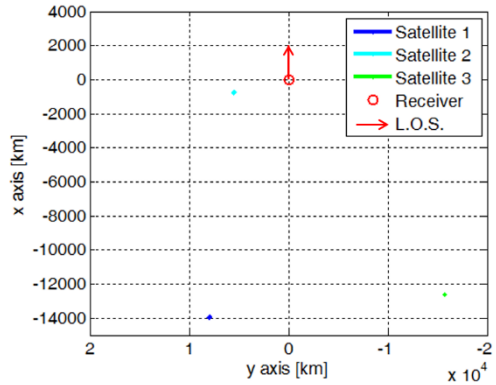

Fig. 5. Trajectories of satellites projected on x-y plane.

As an example Fig. 6 shows the Range-Doppler maps corresponding to the central time batch for the three considered satellites and the red circles indicate the moving target positions. As easily observed the target is completely buried in the disturbance background. After performing TMC and integrating over the available batches results in Fig. 7 are obtained: as evident the time integration largely improves the target to disturbance conditions but, due to the lack of multistatic compensation, the target appears in different Range-Doppler positions. Finally Fig. 8 shows the integrated RD maps obtained with the multistatic compensation step. As evident, also from the smallest frames referring to the same study case but in absence of disturbance, the target position is the same in all integrated maps thus allowing a proper combination of the information coming from the use of the multiple satellites. Just as example Fig. 9 shows the result obtained by conventional non-coherent integration working with intensities with the smallest frames showing a zoom in disturbance free (left) and noisy (right) conditions. With respect to the use of a single transmitter a further improvement is obtained. Obviously, considering the spatial diversity involved by the overall system, also a decentralized approach could be followed performing a first target detection stage for each baseline and then, for each spatial position and each target motion, combining the results in a final detection map by applying a m-out-of-n logic.

5 Conclusion

In this paper a range-Doppler domain processing technique has been proposed able to integrate over long time intervals the returns from a moving target illuminated by multiple GNSS transmitters. This allows the exploitation of the inherent multistatic nature of GNSS-based passive radar in order to increase the detection performance with respect to the single baseline case.

A preliminary analysis conducted on synthetic data considering three GPS satellites has been carried out. The results showed the effectiveness of the proposed technique, thus suggesting the potential of this approach to increase the detection performance by exploiting multiple transmitters and even multiple constellations.

Acknowledgements

This project has received funding from the European GNSS Agency under the European Union's Horizon 2020 programme under grant agreement No 641486, "Galileo-based passive radar system for maritime surveillance — spyGLASS". Project Consortium includes Aster S.p.A. (Italy), University of Rome "La Sapienza" (Italy), University of Birmingham (UK) and Elettronica Gmbh (Germany). The first spyGLASS prototype is an experimental van-mounted system designed and developed by Aster S.p.A. and Elettronica Gmbh.

References

[1] S. Jin, G.P. Feng, S. Gleason, "Remote sensing using GNSS signals: Current status and future directions", *Adv. in Space Res.*, Vol. 47, no. 10, 17 May 2011, pp. 1645-1653.

[2] M. Antoniou, M. Cherniakov "GNSS-based bistatic SAR: a signal processing view", *EURASIP Journal on Advances in Signal Processing*,2013:98.

[3] Q. Zhang, M. Antoniou, W. Chang and M. Cherniakov, "Spatial Decorrelation in GNSS-Based SAR Coherent Change Detection," in *IEEE TGRS*, vol. 53, no. 1, pp. 219-228, Jan. 2015.

[4] F. Santi, M. Antoniou and D. Pastina, "Point Spread Function Analysis for GNSS-Based Multistatic SAR," in *IEEE GRSL*, vol. 12, no. 2, pp. 304-308, Feb. 2015.

[5] F. Santi, M. Bucciarelli, D. Pastina, M. Antoniou and M. Cherniakov, "Spatial Resolution Improvement in GNSS-Based SAR Using Multistatic Acquisitions and Feature Extraction," in *IEEE TGRS*, vol. 54, no. 10, pp. 6217-6231, Oct. 2016.

[6] H. Ma, M. Antoniou, F. Santi, D. Pastina, M. Bucciarelli, F. Pieralice, M. Cherniakov, "Maritime target detection using GNSS-based radar: Experimental proof of concept", to be presented at the *IEEE Radar Conf.*, Seattle, USA, May 2017.

[7] X. He, T. Zeng and M. Cherniakov, "Signal detectability in SS-BSAR with GNSS non-cooperative transmitter," in *IEE Proc. RSN*, vol. 152, no. 3, pp. 124-132, 3 June 2005.

[8] F. Pieralice, F. Santi, D. Pastina, M. Bucciarelli, H. Ma, M. Antoniou, M. Cherniakov, "GNSS-Based Passive Radar for Maritime Surveillance: Long Integration Time MTI Technique", to be presented at the *IEEE Radar Conf.*, Seattle, USA, May 2017.

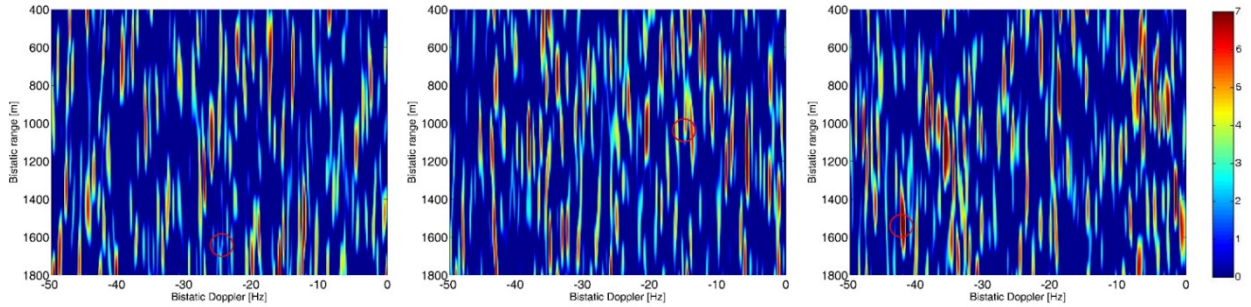

Fig. 6. Range-Doppler maps corresponding to the central time batch for the three considered satellites. The red circle indicates the moving target position.

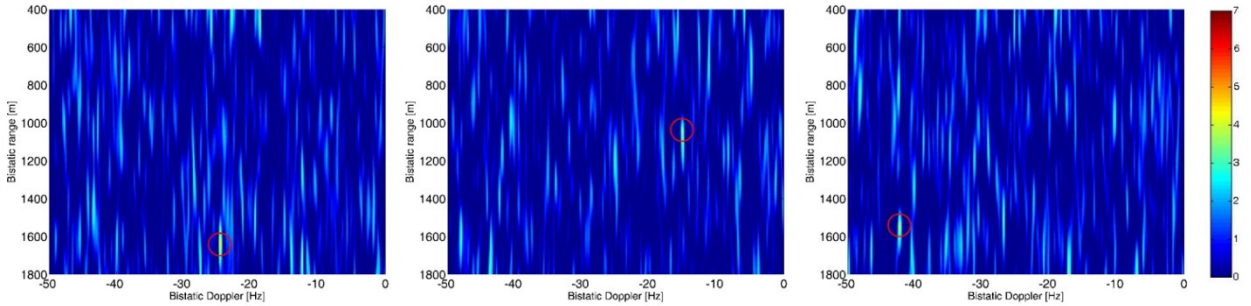

Fig 7. Range-Doppler maps obtained by integrating 15 batches for the three considered satellites without multistatic compesation. The red circle indicates the moving target position.

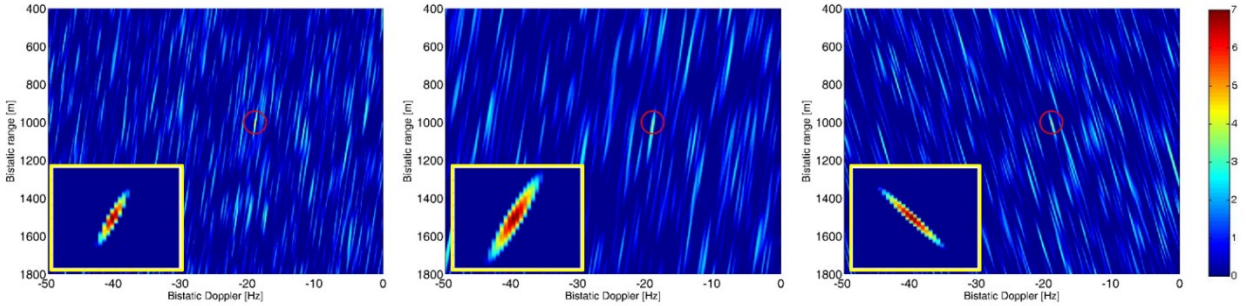

Fig 8. Range-Doppler maps obtained by integrating 15 batches for the three considered satellites with multistatic compesation. The red circle indicates the moving target position.

Parameter	**Value**
Satellites SVID	13, 15, 28
Carrier frequency	1575,42 MHz
Chip rate (C/A code)	1.023 MHz
Code length	1 ms
Target position at u=0	[1000, 0, 0] km
Target velocity	[7.07 7.07 0] kn
Target RCS	15 dB

Table 1 – Simulated scenario parameters.

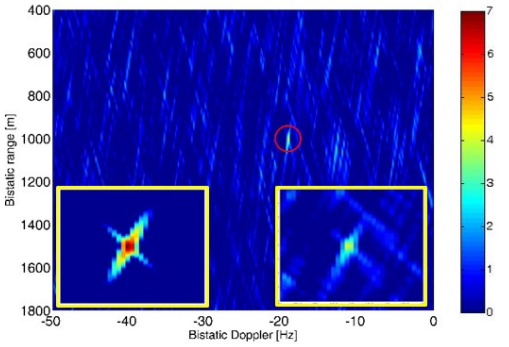

Fig. 9. Summation of RD maps for the three satellites